energy&fuels

Article

pubs.acs.org/EF

Advances in Asphaltene Petroleomics. Part 1: Asphaltenes Are Composed of Abundant Island and Archipelago Structural Motifs

Martha L. Chacón-Patiño,[†] Steven M. Rowland,[*,†,‡] and Ryan P. Rodgers[*,†,‡,§]

[†]National High Magnetic Field Laboratory and [‡]Future Fuels Institute, Florida State University, 1800 East Paul Dirac Drive, Tallahassee, Florida 32310, United States

[§]Department of Chemistry and Biochemistry, Florida State University, 95 Chieftain Way, Tallahassee, Florida 32306, United States

Supporting Information

ABSTRACT: For decades, discussion of asphaltene structure focused primarily on molecular weight. Now that it is widely accepted that asphaltene monomers are between ~250 and 1200 g/mol, disagreement has turned to asphaltene architecture. The classic island model depicts asphaltenes as single core aromatic molecules with peripheral alkyl side chains, whereas the less widely accepted archipelago model, includes multiple aromatic cores that are alkyl-bridged with multiple polar functionalities. Here, we analyze asphaltene samples by positive-ion atmospheric pressure photoionization Fourier transform ion cyclotron resonance mass spectrometry and perform infrared multiphoton dissociation to identify their aromatic core structures to shed light on the abundance of island and archipelago structural motifs. Our results indicate that island and archipelago motifs coexist in petroleum asphaltenes, and unlike readily accessible island motifs, asphaltene purification is required to detect and characterize archipelago species by mass spectrometry. Moreover, we demonstrate that mass spectrometry analysis of asphaltenic samples is biased toward the preferential ionization/detection of island structural motifs and that this bias explains the overwhelming mass spectral support of the island model. We demonstrate that the asphaltene structure is a continuum of island and archipelago motifs and hypothesize that the dominant structure (island or archipelago) depends upon the asphaltene sample.

INTRODUCTION

The evolution of the molecular view of the asphaltene structure is fraught with controversy and inconclusive debates.[1−3] For example, after 40 years of research, asphaltene molecular weight distributions still varied by more than an order of magnitude.[4−10] At some point, the debate focused on whether asphaltenes were monomers or polymers and how that affected molecular weight. Today, the consensus is that asphaltenes are monomeric,[11] and techniques such as time-resolved fluorescence depolarization (TRFD) and mass spectrometry (MS) converged on molecular weights between ~250 and 1200 g/mol, with an average of approximately 750 g/mol.[11−20]

However, disagreement remains on the molecular structure of asphaltene monomers. There are two schools of thought as to the nature of aromatic core organization within asphaltene compounds.[21,22] The classic island architecture, also referred as "like your hand" model, depicts asphaltenes consisting of one aromatic core (the palm) with peripheral alkyl side chains (as fingers).[23] On the contrary, the archipelago model suggests that asphaltenes contain more than one aromatic core linked by alkyl bridges.[24] The island model is rooted in the early 1960s work of Yen and co-workers, who used X-ray diffraction to propose a hierarchical model for the asphaltene structure.[25] Afterward, the widely accepted molecular picture of asphaltenes assumed that most of the aromatic rings were condensed into a single fused core with peripheral alkyl side chains and heteroatomic functionalities. In these structures, π stacking between the aromatic sheets was thought to be the driving molecular interaction for aggregation.[26−28] Since the early 2000s, asphaltene analyses by direct molecular imaging,[29] fluorescence depolarization,[7,30] and MS/tandem MS[31−33] have strengthened the hypothesis of the dominance of island structures in petroleum asphaltenes.

Asphaltenes Are Island. Direct molecular imaging by atomic force microscopy (AFM) suggests that only one polycyclic aromatic hydrocarbon (PAH) core, made up of ~7 fused rings, is the dominant structure in asphaltenes.[34] According to Groenzin and Mullins, this molecular motif is in agreement with the known molecular weights for petroleum asphaltenes and the results from TRFD.[7] In TRFD studies, both island model compounds and petroleum asphaltenes exhibit similar rotation times. Thus, asphaltenes are island. Several MS reports by Pomerantz and co-workers[35] and Kenttämaa and co-workers[36] further support the predominant structure of only one PAH per asphaltene molecule. In the case of Pomerantz and co-workers, two-step laser desorption/ionization mass spectrometry (L^2MS) is chosen to analyze asphaltene samples because of its proposed ability to suppress plasma-phase aggregation.[14,35,37] Since 2008, this technique was employed to measure monomeric molecular weight distributions (MWDs) for asphaltenes, which range between ~350 and 1200 Da, with a broad maximum near 600 Da. With regard to the asphaltene structure, L^2MS analysis of asphaltene model compounds demonstrated that archipelago structures undergo extensive fragmentation as a result of cleavage of alkyl bridges, even at low laser energies (~3.5 mJ).[35] On the other hand, island compounds only exhibit mass loss that corresponds to fragmentation of alkyl side chains. Similarly, other publications

Received: September 22, 2017
Revised: November 2, 2017
Published: November 8, 2017

DOI: 10.1021/acs.energyfuels.7b02873
Energy Fuels 2017, 31, 13509−13518

demonstrated that the variation of the laser power in the MS analysis of asphaltenes did not produce extensive fragmentation. These results were considered unquestionable evidence for the dominance of island structural motifs in asphaltenes.[35,38]

Additional MS reports on the behavior of virgin asphaltenes in unimolecular decomposition studies (tandem MS) by laser-induced acoustic desorption (LIAD) coupled to electron impact ionization indicate a predominance of island motifs.[36] Kenttämaa and co-workers[31] traced the fragmentation behavior of seven asphaltene samples from different geological origins, including Maya and Surmont asphaltenes. Regardless of geological origin and molecular weight, all asphaltene ions preferentially exhibited fragmentation pathways that correlated to island motifs, where the mass losses indicated only cleavage of alkyl side chains. In this report, the authors concluded that the minimum core size for asphaltenes is 4 fused aromatic rings and that high-molecular-weight asphaltenes are a result of increased alkyl side-chain content.[31]

Recently, Schuler et al.[29] used AFM and scanning tunneling microscopy to reveal the structure of more than 100 asphaltene molecules derived from UG8 Kuwait crude oil. The structures found in this study demonstrate that asphaltenes are ultra-complex mixtures that exhibit a wide diversity of molecular motifs. The results highlight the predominant detection of island-type motifs, including highly peri- and cata-condensed PAH structures with five-membered rings within the cores. This work also demonstrated the first direct observation of few archipelago-type structures but with bridges no longer than one single bond.

Asphaltenes Must Be Island and Archipelago. Despite all of the support for island motifs as the dominant architecture of petroleum asphaltenes, the model has several fundamental flaws. Many comprehensive works suggest that asphaltenes exhibit a series of properties that are not explained by the island model.[36−39] Such properties include heterogeneous aggregation of asphaltenes,[40] occlusion of saturates and alkyl aromatic compounds inside asphaltene networks,[41,42] extensive solvent entrainment,[43] and the chemistry of the upgrading products (e.g., hydroprocessing, thin-film pyrolysis, and thermal cracking).[4,44] In thermal cracking and thin-film pyrolysis, asphaltenes produce a wide diversity of gas (e.g., H_2S, CO_2, CH_4, and C_2H_6), liquid, and solid (coke, insoluble in both heptane and toluene) products.[45] Liquids, usually referred to as distillables, can be fractionated into compounds that are *n*-heptane-soluble (produced maltenes) and compounds that are *n*-heptane-insolubles but toluene-solubles (residual asphaltenes). Several reports on the molecular characterization of the distillable products from asphaltene thermal cracking indicate substantial production of 1−4-ring alkyl aromatics.[44,46−48] Collectively, these observations challenge the hypothesis of the island model as the sole or even the dominant structural motif. If asphaltenes are dominated by an island-type architecture, the products of thermal cracking processes would be coke, light-naphtha-range alkanes, and gases, which they clearly are not.[49−51] The fact that asphaltene samples from diverse geological origins yield different amounts of coke under the same pyrolysis conditions (from ∼10 to ∼75 wt %) indicates that these complex samples exhibit a wide diversity of molecular motifs.[52−55] We hypothesize that the predominance of island or archipelago motifs depends upon the asphaltene sample and is of paramount importance, because the quantitation of these motifs in crude oils should be an accurate method to predict yields/optimal conditions for upgrading heavy feedstocks and, ultimately, process-dependent economic value.

The use of thermal cracking as a tool for quantification of archipelago and island structures in petroleum is a challenge because of the need to minimize secondary reactions between the primary cracked products. However, Gray and co-workers[56,57] demonstrated that thin-film pyrolysis yields undeniable evidence of the high concentration of bridged structures in asphaltenes from diverse geological origins (i.e., Maya, Athabasca, and Cold Lake).[56,57] Mass balance results and analysis of the liquid products by nuclear magnetic resonance (NMR) and gas chromatography demonstrate the complexity of the aromatic products. The molecular composition of the produced liquids indicates a high concentration of 1−4+-ring aromatics, thiophenes, and naphthenobenzothiophenes. This complexity is the result of the high abundance of aromatic cores linked by alkyl bridges. Despite the evidence, several reports indicate that the data from bulk decomposition studies are easily misinterpreted as a result of secondary reactions.[13,26,58]

To the best of our knowledge, the most ideal way to perform molecular-level decomposition studies is by MS. Mass specrometric analyses provide the ability to isolate small fractions of asphaltene ions based on their molecular weight (m/z), and decomposition under high vacuum (10^{-10} Torr) ensures that the probability of secondary reactions is extremely low. Infrared multiphoton dissociation (IRMPD) followed by ion cyclotron resonance MS has proven useful to understand building blocks in complex mixtures.[59,60] Podgorski et al.[61] showed evidence of archipelago structures in deasphalted heavy distillate [atmospheric equivalent boiling point (AEBP) of 523−593 °C] from a DISTACT distillation by Fourier transform ion cyclotron resonance mass spectrometry (FT-ICR MS) with IRMPD. Samples were separated on the basis of the number of fused aromatic rings, and observation of archipelago structures was most obvious in the analysis of the 4- and 5-ring fractions. Parent ions isolated from the 5-ring fraction were centered about double bond equivalents (DBE) of ∼21, and abundant fragment ions were detected as low as DBE of 7. This data provides clear evidence of archipelago structures in heavy distillates. The work also presented results from *n*-pentane (C_5) maltenes and asphaltenes isolated from the *n*-heptane deasphalted oil. The results revealed that the C_5 asphaltene fragment ions were enriched in low DBE structures (archipelago), whereas the C_5 maltenes were enriched in fragments with DBE of >20 (island).[61]

Here, we address the inconsistency of mass spectral results in the structural analysis of asphaltenes in hopes to reveal the reason behind the pervasive (but incorrect) hypothesis that all asphaltene samples are predominately composed of island structural motifs. C_5, C_{5-6}, and C_7 asphaltenes were isolated from a South American heavy oil, and entrained maltenes (co-precipitants) were successively removed by a purification process reported elsewhere.[41] The asphaltene samples, before and after purification, were analyzed by FT-ICR MS and subjected to IRMPD experiments to reveal the aromatic core building blocks, to assess the importance of co-precipitant removal in mass spectrometric structural analysis of asphaltenes. IRMPD results indicate that island and archipelago structures coexist in petroleum asphaltenes and that the wide range of monomer ion yields exhibited by the compounds in asphaltenes limit their complete characterization. Specifically, our results indicate that island structural motifs ionize more efficiently than archipelago structures, most likely as a result of

DOI: 10.1021/acs.energyfuels.7b02873
Energy Fuels 2017, 31, 13509−13518

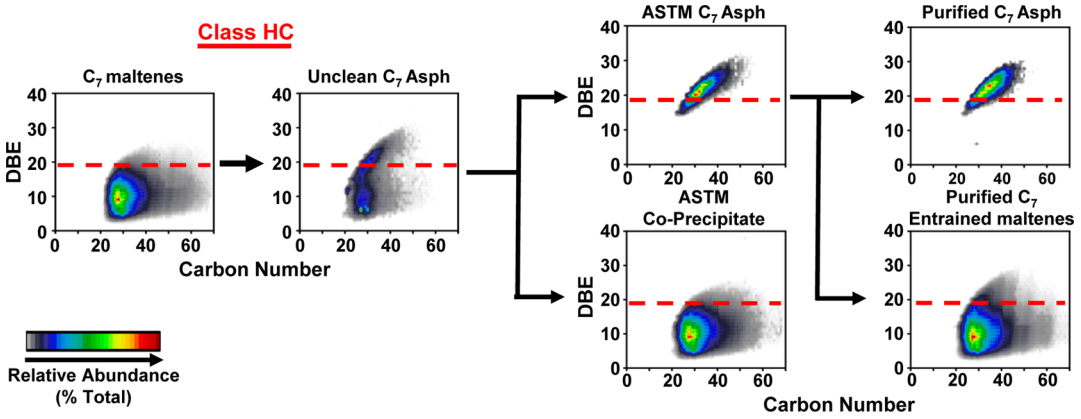

Figure 1. Isoabundance color-contoured plots of DBE versus carbon number for the hydrocarbon class from maltenes, co-precipitate wash, entrained maltenes, and unclean C_7, ASTM C_7, and purified C_7 asphaltenes.

increased aggregation of archipelago structures that thus limits their monomer ion yield. Thus, selective separation of island compounds is of paramount importance to extend the characterization of asphaltenes and detect archipelago species.

EXPERIMENTAL SECTION

Materials. Analyses were conducted with asphaltenes from a South American heavy oil [American Petroleum Institute (API) gravity of 14.2°]. High-performance liquid chromatography (HPLC)-grade *n*-heptane (C_7), *n*-pentane (C_5), and toluene (J.T. Baker Chemicals, Phillipsburg, NJ, U.S.A.) and Whatman 2 filter paper (30 μm, 150 mm diameter, GE Healthcare Bio-Sciences, Pittsburgh, PA, U.S.A.) were used as received. Asphaltene model compounds, coronene, perylene, dibenzo[*a*,*h*]anthracene, pentacene, truxene, benzo[*k*]fluoranthene, and rubrene, were purchased from Sigma-Aldrich (St. Louis, MO, U.S.A., purity of ≥99.0%). Model compounds provided by Murray R. Gray, named as ABA, DDP, and chol-thiophene, are reported elsewhere.[62]

Asphaltene Precipitation Process. Figure S1 of the Supporting Information illustrates the sample preparation procedure with gravimetric results. Asphaltenes were precipitated following a modified ASTM D6560-12 method. Crude oils (~10 g) were sonicated (Branson Ultrasonics, Danbury, CT, U.S.A., 22 kHz and 130 W) at 60 °C as 400 mL of *n*-heptane was added dropwise over a 2 h period. The mixture was allowed to stand for 24 h, and solids (unclean asphaltenes) were separated from C_7 maltenes by filtration (Whatman grade 42) and washed in a Soxhlet extractor with C_7 for 120 h. C_7 asphaltenes were recovered by dissolution in hot toluene (~98 °C), which was evaporated under nitrogen to yield solid ASTM C_7 asphaltenes. Subsequently, C_7 asphaltenes were purified by further extraction of occluded maltenes, following a procedure published elsewhere.[41] C_5 asphaltenes were prepared as described above. As a result, unclean C_5 asphaltenes, ASTM C_5 asphaltenes, and purified C_5 asphaltenes were obtained. Additionally, 0.2 g of purified C_5 asphaltenes was washed with *n*-heptane for 72 h to extract C_{5-6} asphaltenes. The samples were dried under N_2, weighed, and stored in the dark to avoid photooxidation. This procedure was repeated in triplicate.

Positive-Ion Atmospheric Pressure Photoionization [(+)APPI] FT-ICR MS. Samples were dissolved in toluene at a concentration of 200 μg mL^{-1} and directly infused at 50 μL min^{-1}. A Thermo-Fisher Ion Max APPI source (Thermo-Fisher Scientific, Inc., San Jose, CA, U.S.A.) was operated with a vaporizer temperature of 350 °C. N_2 sheath gas was operated at 50 psi, and N_2 auxiliary gas (32 mL min^{-1}) helped prevent sample oxidation. Gas-phase neutrals were photoionized by a 10 eV (120 nm) ultraviolet krypton lamp (Syagen Technology, Inc., Tustin, CA, U.S.A.). Samples were analyzed with a custom-built passively shielded 9.4 T FT-ICR mass spectrometer equipped with a 22 cm horizontal room-temperature bore.[63] Time-domain transient signals (6.2 s) were collected and processed by a modular ICR data acquisition system (Predator).[64] Positive ions were accumulated externally for 100−3000 ms in the second radio frequency (rf)-only octopole and collisionally cooled with helium prior to transfer through a rf-only octopole to a seven-segment, open cylindrical cell with capacitively coupled excitation electrodes. Chirp excitation (~1400−70 kHz at a sweep rate of 50 Hz μs^{-1} and 360 V_{p-p} amplitude) accelerated the ions to a detectable cyclotron radius. Approximately 75−200 (APPI) time-domain acquisitions were co-added, Hanning-apodized, and zero-filled once before Fourier transform and magnitude calculation. Frequency was converted to m/z by the quadrupolar electric trapping potential approximation. Spectra were internally calibrated from an extended homologous alkylation series of high relative abundance before peak detection [>6σ baseline root-mean-square (RMS) noise] and automated elemental composition assignment.

Mass Isolation and Fragmentation Analysis. Mass segments (4 Da wide) were isolated by a mass-resolving quadrupole prior to external ion accumulation and subsequently transferred to the FT-ICR cell for mass measurement and dissociation. IRMPD (λ = 10.6 μm, 40 W, 50−4000 ms irradiation, Synrad CO_2 laser, Mukilteo, WA, U.S.A.) was performed to fragment the mass-isolated segments in the FT-ICR cell. All molecular formula assignments and data visualization were performed with PetroOrg software.[65]

RESULTS AND DISCUSSION

Asphaltene Purification. The work presented here aims to highlight the importance of solvent cleaning, previously reported by Chacón-Patiño et al.[41] and Alboudwarej et al.,[66] and solvent selection in the precipitation/subsequent analysis of asphaltenes, especially by MS. Figure 1 shows the isoabundance color-contoured plots of DBE versus carbon number for the hydrocarbon (HC) class from maltenes and unclean C_7, ASTM C_7, and purified C_7 asphaltenes as well as the co-precipitate wash and entrained maltenes for each purification step. It is readily apparent that the maltenes and asphaltenes occupy very different compositional space within the DBE versus carbon number plots.[16] However, the unclean asphaltenes show a bimodal distribution, with both maltene and asphaltene contributions. This is due to the presence of co-precipitated maltenes (co-precipitates) that precipitate along with the asphaltene molecules. After the first step of Soxhlet extraction with *n*-heptane (top right in Figure 1), we observe that the washing step removed the low DBE maltenes from the ASTM C_7 asphaltenes, which are concentrated in the ASTM co-precipitate fraction (first co-precipitant fraction). Further purification, according to previously published work,[41] was conducted by grinding ASTM asphaltenes and cleaning by

DOI: 10.1021/acs.energyfuels.7b02873
Energy Fuels 2017, 31, 13509−13518

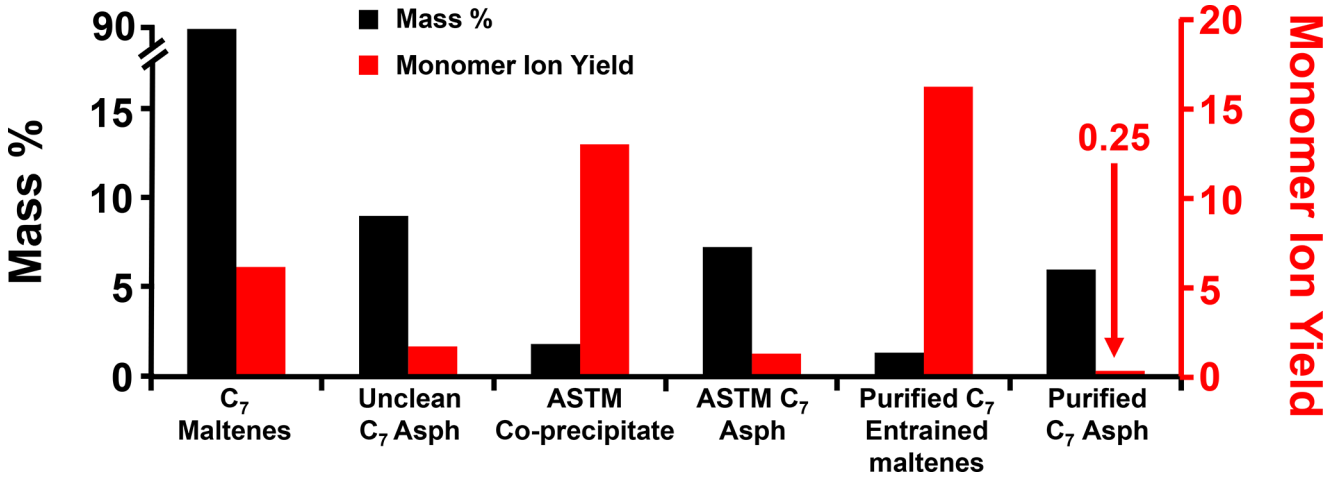

Figure 2. Mass yield and monomer ion yield for C_7 maltenes, co-precipitate wash, entrained maltenes, and unclean C_7, ASTM C_7, and purified C_7 asphaltenes.

additional Soxhlet extraction with *n*-heptane. This purification process results in purified C_7 asphaltenes and a second co-precipitate fraction (entrained maltenes). The two co-precipitate fractions closely resemble species observed in the C_7 maltene sample (far left in Figure 1). The importance of the co-precipitated asphaltenes becomes more evident when we look at the mass yields and associated monomer ion yields for all fractions. Figure 2 shows a bar graph where each black bar equals the mass yield (in weight percent) of each fraction. The initial precipitation of asphaltene yields 90.8% of the mass in maltenes and 9.2% of the mass in the asphaltenes (unclean C_7 asphaltenes). However, upon initial purification of the unclean C_7 asphaltenes, 20% of the unclean asphaltenes are, in fact, maltenes (ASTM co-precipitate) that are removed by heptane extraction. Another 14% are removed (as purified C_7 entrained maltenes) in the second purification step. Thus, the initial 9.2 wt % of asphaltenes dropped yields only 6.1 wt % purified asphaltenes; greater than $^1/_3$ of the initial asphaltene drop mass is co-precipitated/entrained maltenes. This is extremely important, especially when using bulk measurements, such as elemental ratios, NMR, and fluorescence techniques, because maltenes are known to have much lower aromaticity (higher H/C ratio) and are comprised predominately of island structural motifs.[61] The importance in mass spectral analyses is discussed below.

Monomer Ion Yield. Analysis of asphaltenes by MS is especially compromised by the presence of maltenes in supposedly "clean" asphaltene fractions. We now know that one difficulty in the analysis of asphaltenes by MS arises from the drastic differences in ionization efficiencies between maltenes and asphaltenes (red bars in Figure 2). It is thought that difficulties in ionization and detection of asphaltene monomers are due to aggregation of asphaltene molecules prior to and during the ionization process, rather than the ionization potential of any given asphaltene monomer.[16] It is likely that asphaltene monomers alone have relatively similar ionization potentials. However, aggregation of asphaltenes during the ionization process results in reduced ion signal from monomeric (non-aggregated) asphaltenes. This hypothesis is supported by previous work,[16] where asphaltenes were shown to aggregate during electrospray ionization at concentrations as low as 50 μg mL^{-1}. Equation 1 is used to calculate the monomer ion yield (MIY) for the maltenes, asphaltenes, and co-precipitated samples, where t_a is the time required to accumulate a target number of ions prior to mass spectral analysis.

$$\text{monomer ion yield} \propto \frac{1}{t_a} \tag{1}$$

The monomer ion yield may be thought of as the inverse of the time needed to acquire a target number of ions at a given sample concentration. For these experiments, we held all sample concentrations constant and varied the ion accumulation time to provide an approximately constant ion number. Therefore, the monomer ion yield, or the efficiency with which monomer asphaltene ions are produced, is inversely proportional to the ion accumulation time. This measurement provides an indication of the ease of detection for monomeric ions for each sample. Figure 2 shows the monomer ion yield for each sample. The monomer ion yield of asphaltene samples is much lower than that of the maltenes and co-precipitates and is shown to decrease for asphaltene samples with extended solvent purification. The final purified C_7 asphaltenes exhibit a ~50-fold lower monomer ion yield when compared to the co-precipitates, despite accounting for 67 wt % (6.1 wt %) of the initial asphaltene mass (9.2 wt %). Two important conclusions can be drawn from this data. First, unclean C_7 asphaltenes were comprised of ~33% co-precipitated maltenes, which exibited the greatest monomer ion yield; however, the monomer ion yield of the unclean asphaltene sample is approximately equal to the ASTM asphaltenes. This indicates that, even in the presence of ~33% entrained maltenes (co-precipitated maltenes), the ionization of the total sample is still poor, which suggests that aggregation is the prevailing factor for poor ionization of asphaltene monomers. Second, the purified C_7 asphaltenes, which are the largest mass percentage of the initial unclean asphaltenes (~67%), exhibit the lowest monomer ion yield and ionize ~50 times less efficiently than co-precipitated maltenes. For this reason, sample preparation techniques are imperative to the analysis of asphaltenes, especially at the molecular level.

Pentane versus Heptane Asphaltenes. In addition to appropriate solvent cleaning, the solvent selection for asphaltene precipitation plays a major role in the composition of asphaltene samples. For these experiments, we isolated the *n*-pentane-insoluble asphaltenes, purified them with *n*-pentane

DOI: 10.1021/acs.energyfuels.7b02873
Energy Fuels 2017, 31, 13509−13518

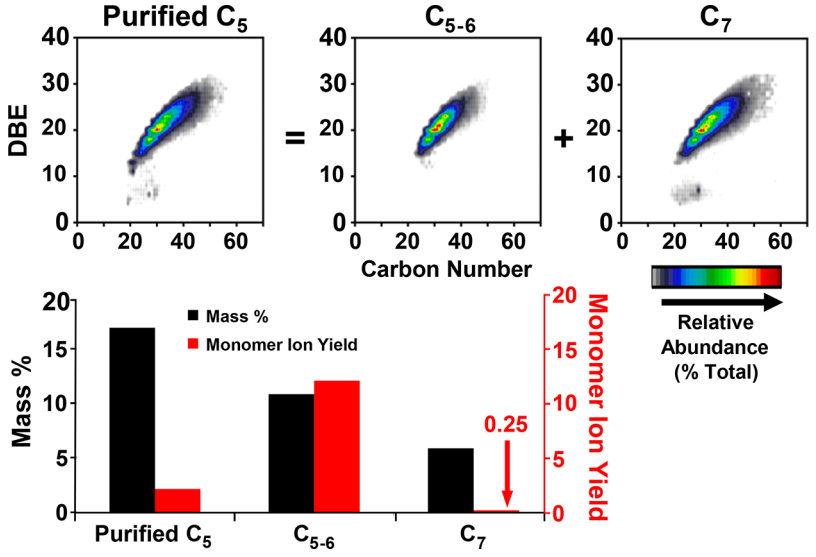

Figure 3. (Top) DBE versus carbon number plots for the C_5, C_{5-6}, and C_7 asphaltenes and (bottom) mass percentages and monomer ion yield for each sample.

according to the previously discussed method, and carried out Soxhlet extraction of the purified C_5 asphaltenes with *n*-heptane. This procedure results in three samples: purified C_5 asphaltenes (C_5 insoluble), C_{5-6} asphaltenes (C_5 insoluble and C_7 soluble), and C_7 asphaltenes (C_7 insoluble). By this methodology, C_5 asphaltenes are a mixture of C_{5-6} and C_7 asphaltenes. Figure 3 summarizes the DBE versus carbon number plots for the HC class of C_5, C_{5-6}, and C_7 asphaltenes as well as the mass percentages and monomer ion yield for each sample. Although the compositional space for all three samples is relatively similar, we again observe extreme differences in the monomer ion yield. Not only are the C_{5-6} asphaltenes approximately 65% of the mass of the purified C_5 asphaltenes, but the monomer ion yield of C_{5-6} is ~50-fold greater than that of C_7 asphaltenes. The differences in mass percent and ion production suggest that, although purified C_5 asphaltenes are composed of an approximately 2:1 ratio of C_{5-6}/C_7, we preferentially observe C_{5-6} asphaltene ions during MS analysis of C_5 asphaltenes. Given that both samples occupy very similar compositional space, what accounts for their vastly different monomer ion yields? This point will become more significant and addressed in the discussion of structural motifs, below.

Determination of Island versus Archipelago Motifs. Determining the structural motifs, island versus archipelago, is an extremely difficult task and one that has been the subject of continued debate. Techniques such as NMR and fluorescence depolarization are bulk measurements that may be skewed on the basis of several factors, including sample preparation. Recently, direct molecular imaging by AFM has proven useful in understanding the chemical structures of asphaltenes as a result of its ability to image single asphaltene molecules,[29,67] and both island and archipelago structures have been proposed on the basis of AFM data. FT-ICR MS is uniquely suited to understand the structural composition of asphaltenes because the molecular-level information obtained by FT-ICR MS, in conjunction with the ability to perform in-cell ion fragmentation, provides useful insight into the structural motifs. Fragmentation of asphaltenes by IRMPD results in two primary fragmentation pathways. The first consists of dealkylation; it is observed primarily in alkylated, single-core PAH compounds, which are island-type asphaltenes. In this case, there is a decrease in the number of carbon atoms in the IRMPD fragments with no decrease in aromaticity (DBE). The second fragmentation pathway involves the cleavage of alkyl or cycloalkyl bridges that link multiple aromatic cores. These archipelago-type compounds result in fragments that exhibit both a loss of carbon number and a loss of aromaticity (DBE). Figure 4 shows the fragmentation spectra for select model asphaltene compounds used in this study. Benzo[*a*]-phenanthrene, DDP, and truxene serve as examples of island model compounds, whereas ABA, chol-thiophene, and rubrene serve as examples of archipelago model compounds. It is

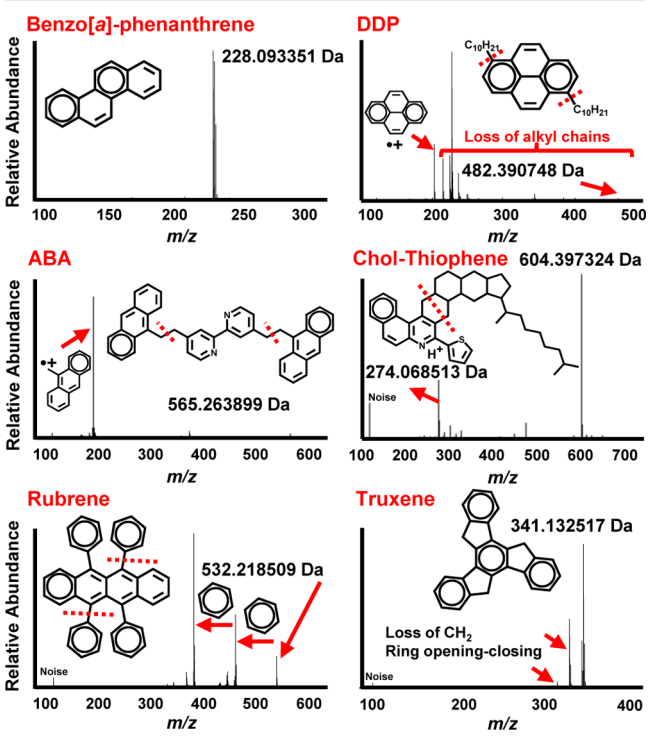

Figure 4. Fragmentation spectra (IRMPD of 1000 ms) for island-type model compounds benzo[*a*]phenanthrene, DDP, and truxene and archipelago-type model structures ABA, chol-thiophene, and rubrene.

DOI: 10.1021/acs.energyfuels.7b02873
Energy Fuels 2017, 31, 13509−13518

important to highlight that, under the irradiation times that were used in this study, fragmentation across the aromatic cores is not observed. Cata-condensed PAH cores exhibited only loss of H_2, which was previously reported by collision-induced dissociation (CID)[62] and leads to an increase in DBE of 1. Truxene (single core that contains five-membered rings) exhibits the most notable change to the core; in this case, it undergoes a ring-opening/-closing event with a loss of CH_2. However, this fragmentation pathway does not change the DBE of the molecule. Also, two important points to note here are the observations of cleavage across cycloalkyl rings in chol-thiophene and the cleavage of phenyl groups from rubrene. Questions have arisen in the past as to whether or not these bonds fragment during IRMPD. We have definitively shown that these bonds will, in fact, fragment under the given conditions and that the type of fragmentation depends upon the structure.[68] Figures S2–S6 of the Supporting Information include the mass spectra of several model compounds by IRMPD under irradiation times between 50 and 4000 ms. The aromatic cores of island compounds, with peri- and cata-condensed structures are shown to be highly stable under these conditions.

Before the discussion of fragmentation data from asphaltene samples, we must address the fragmentation products of both island and archipelago structural motifs that contain multiple functionalities within the core structures. Figure 5 shows

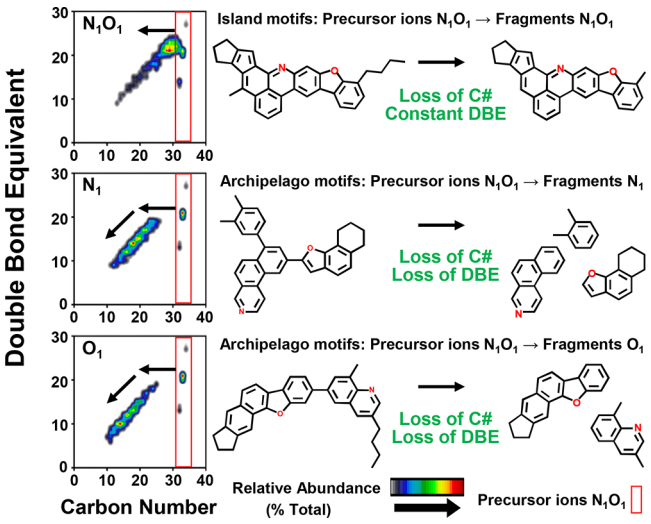

Figure 5. Theoretical structures for the most abundant N_1O_1 parent ions with fragmentation routes that correlate with (top) island and (middle and bottom) archipelago structural motifs.

proposed theoretical structures that correspond to the most abundant parent ions for the N_1O_1 class with both island and archipelago structural motifs and the corresponding experimental fragments from IRMPD. The DBE versus carbon number plots show experimental fragments from FT-ICR MS analysis of C_7 asphaltenes, and the model structures drawn for N_1O_1 compounds (right side of Figure 5) reflect the molecular compositions from parent ions and structures based on those reported by direct molecular imaging.[29,67] The fragmentation of island-type compounds results in the simple loss of alkyl side chains. By this fragmentation pathway, a parent ion with a starting heteroatom class of N_1O_1 produces an N_1O_1 fragment with either the same DBE or an increase in DBE of 1 as a result of the loss of H_2 (through ring opening/closing) (top in Figure 5). Two archipelago scenarios (middle and bottom in Figure 5) are also shown, where the heteroatoms are located in different aromatic cores. In this type of fragmentation, several types of fragments may be produced and it is possible for the charge to stay with either of the heteroatoms (or potentially with a fragment that possesses no heteroatom, which results in a hydrocarbon fragment). For all scenarios, the observed loss in DBE is indicative of archipelago structural motifs. The DBE versus carbon number plots clearly show the predominance of high DBE compounds in the island N_1O_1 fragments (top), which are contrary to the lower DBE fragments of the N_1 (middle) and O_1 (bottom) fragments. We should also point out that not all N_1O_1 fragment ions reveal island structural motifs. We observe N_1O_1 fragments down to C_{12} DBE of 9, which indicates a 3-ring aromatic with both nitrogen and oxygen functionalities present in a single core. These fragments are the products of archipelago structures, likely from N_xO_y or $N_xO_yS_z$ parent ions.

IRMPD Fragmentation of Asphaltenes. Prior to fragmentation with IRMPD, a 4 Da mass distribution from m/z 454 to 458 was isolated with a mass resolving quadrupole. The ions present within the mass range were irradiated for 1000 ms by IRMPD, and the resulting fragments were detected by FT-ICR MS. Figure 6 shows the IRMPD fragmentation mass spectra (top) as well as the DBE versus carbon number distributions for the purified C_5, C_{5-6}, and C_7 asphaltenes. For purified C_5 and C_{5-6} asphaltenes, the most abundant fragment ions show successive loss of CH_2 units (~14 Da mass losses), as previously shown by Kenttämaa and co-workers,[31−33,36,69] without significant loss of aromaticity, indicative of island-type structures. However, C_7 asphaltenes show a bimodal distribution of fragments with the higher masses, from m/z ~300 to 450, corresponding to dealkylation (island), and the lower mass fragments, from m/z ~100 to 300, are indicative of dealkylation and loss of aromaticity (archipelago). The DBE versus carbon number plots (bottom) for the HC classes show the parent ions (prior to fragmentation), located within the red boxes, overlaid with fragment ions (those outside the red boxes). Here again, we see that purified C_5 and C_{5-6} asphaltenes show primarily the presence of high DBE fragments produced from island structures, whereas the abundant C_7 asphaltene fragments are at much lower DBE values, which reveals a greater relative abundance of archipelago structures. For better visualization, Figure 7 summarizes the compositional data (of bottom in Figure 6) into bar graphs of relative abundance versus DBE values for parent and fragment ions from purified C_5, C_{5-6}, and C_7 asphaltenes. The gray portion of the bar is the summed relative abundance of all fragment ions at each DBE value, and the red portion is the summed relative abundance for all parent ions at each DBE value. The total bar height is the total abundance of parent and fragment ions. For example, DBE of 26 is the most abundant DBE value in the purified C_5 asphaltenes. The gray portion of the bar is ~5% relative abundance, and the total bar height is ~17% relative abundance. This means that the fragment ions are present at ~5% relative abundance and the parent ions are present at ~12% relative abundance for DBE of 26. Analysis of the C_5 and C_{5-6} asphaltenes reveals greater relative abundances for parent ions with DBE of <25 when compared to C_7, and the majority of fragment ions are distributed between DBE of 18 and 27. This is contrary to purified C_7 asphaltenes, where the parent ion distributions are all less than 1.5% relative abundance for DBE values of <25 and where the distribution of fragment ions

DOI: 10.1021/acs.energyfuels.7b02873
Energy Fuels 2017, 31, 13509−13518

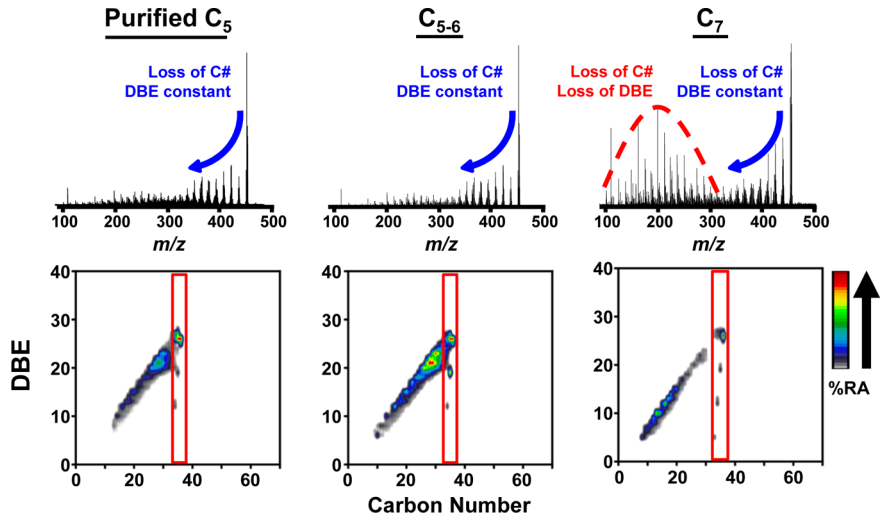

Figure 6. (Top) IRMPD fragmentation mass spectra and (bottom) DBE versus carbon number plots for purified C_5, C_{5-6}, and C_7 asphaltenes.

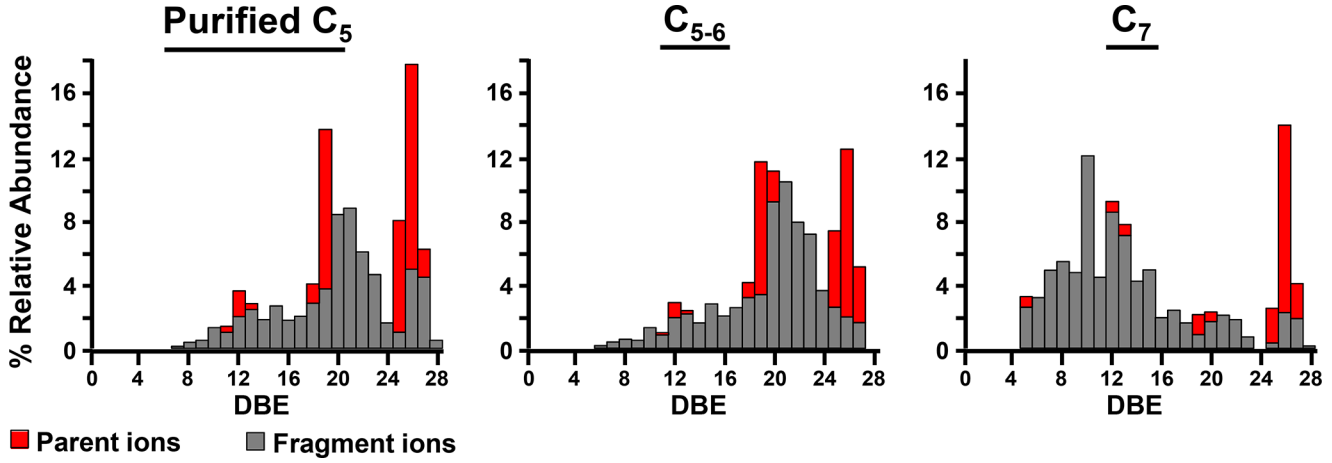

Figure 7. Bar graphs of relative abundance versus DBE values for parent ions (red portion) and fragment ions (gray portion) from purified C_5, C_{5-6}, and C_7 asphaltenes.

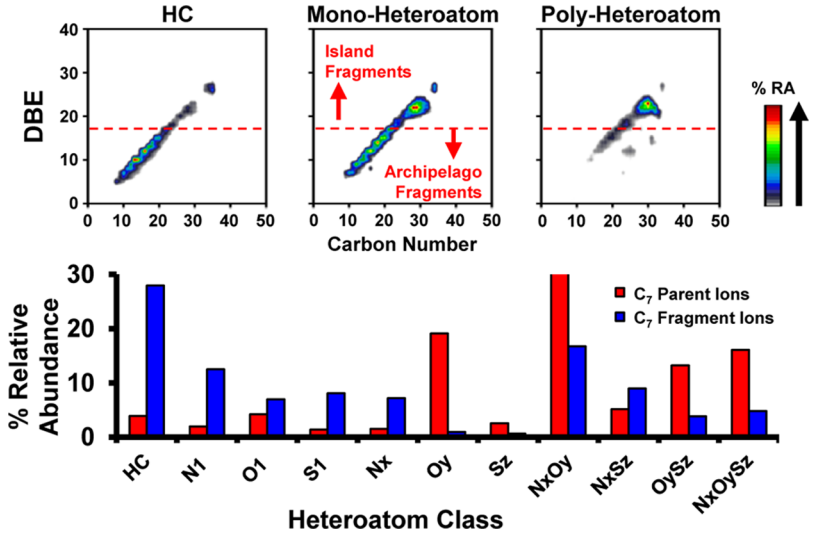

Figure 8. (Top) DBE versus carbon number plots for the HC and mono- and poly-heteroatomic fragments and (bottom) heteroatom class distribution for the parent ions and fragments from purified C_7 asphaltenes.

is most abundant from DBE of 4 to 15. We also observe in C_7 asphaltenes that the most abundant fragments correspond to DBE of 10, 12, and 13, which are indicative of commonly observed asphaltene building blocks, such as phenanthrene,

DOI: 10.1021/acs.energyfuels.7b02873
Energy Fuels 2017, 31, 13509−13518

benzo[*a*]fluorene, and chrysene. In fact, these building blocks match the molecular structure of the archipelago-type asphaltenes recently reported by direct molecular imaging.[29,67]

Until now, we have discussed a small fraction of the ions observed for asphaltene samples. However, to properly understand the entire composition, we must consider all heteroatomic species. Figure 8 shows the heteroatom class distribution (bottom) for the purified C_7 asphaltenes, where the red bars are the summed relative abundance from quadrupole isolated parent ions from m/z 454 to 458 and the blue bars are the summed relative abundance of the fragment ions generated from IRMPD fragmentation of the mass segment mentioned above. Each mass spectral assignment was sorted by heteroatom class and grouped on the basis of heteroatom content into classes that include hydrocarbons (HC), mono-heteroatomic compounds (N_1, O_1, and S_1), and poly-heteroatomic species (ions having more than one heteroatom and denoted as N_x, O_y, S_z, N_xO_y, N_xS_z, O_yS_z, and $N_xO_yS_z$, e.g., N_2, N_3, O_2, O_3, S_2, S_3, N_1O_2, and $N_1O_1S_1$). We see that the parent ions are enriched in poly-heteroatomic species; however, after IRMPD, we observe a shift in relative abundance to favor hydrocarbons and mono-heteroatomic classes. This is due to the fragmentation of poly-heteroatomic archipelago parent ions to produce lower carbon number and lower DBE fragment ions with fewer heteroatoms. The top in Figure 8 also shows the DBE versus carbon number plots for the hydrocarbon fragments as well as the combined plots of mono- and poly-heteroatomic fragments. The red line at DBE of 17 is the boundary defined to identify island versus archipelago fragments. The boundary is determined by subtracting the weighted standard deviation from the weight-averaged DBE value for all assigned parent ions (weight-averaged DBE of 21 ± 4). We conclude that fragment ions with DBE of 17 or less are most likely produced from the fragmentation of archipelago compounds and that fragment ions with DBE greater than 17 are most likely island fragments. The HC class DBE versus carbon number plots reveal that the majority of the hydrocarbon fragments are derived from archipelago structures, whereas mono-heteroatomic fragments are composed of a more evenly distributed mixture of island and archipelago structures. Finally, the poly-heteroatomic fragment ions are composed of primarily island-type ions. These results indicate that the surviving poly-heteroatomic compounds are island; however, this observation does not rule out the existence of archipelago poly-heteroatomic species. The fact that we observe a decrease in the relative abundance of poly-heteroatomic ions and a subsequent increase in HC and mono-heteroatomic classes in the class graph (bottom in Figure 8) suggests the fragmentation of archipelago poly-heteroatomic ions form fragment ions with lower numbers of heteroatoms. It is difficult to comment on the quantity of island versus archipelago structures from the work presented here, but we can conclude that island and archipelago structures coexist in petroleum asphaltenes and that archipelago structures likely play a greater role than previously thought.

CONCLUSION

The removal of co-precipitated maltenes from C_7 asphaltenes is paramount for their mass spectral analysis and enabled direct identification of abundant archipelago structural motifs. The co-precipitates are especially problematic, because they were found to have a >50-fold higher monomer ion yield than the purified asphaltene. Thus, failure to remove these maltenic species greatly affects subsequent compositional and structural analyses. Purified C_5 asphaltenes exhibit a ∼10-fold increase in the monomer ion yield compared to purified C_7 asphaltenes and yield similar compositional results (in carbon number and DBE). However, removal of the C_7-soluble fraction from purified C_5 asphaltenes revealed that this fraction, C_{5-6} asphaltenes, accounted for the increased monomer ion yield. The extreme differences in C_5, C_{5-6}, and C_7 asphaltene monomer ion yields, despite their near identical carbon number and DBE distributions, is explained by IRMPD fragmentation. C_5 asphaltene is a mixture of C_{5-6} and C_7 asphaltenes. C_{5-6} asphaltene is comprised predominately of island-type architecture, whereas C_7 asphaltene reveals a mixture of island and archipelago motifs. Fragmentation of the C_5 asphaltene (C_{5-6} + C_7) sample shows almost exclusively island-type fragments (as a result of the 50-fold higher ionization efficiency of C_{5-6} asphaltenes relative to C_7), despite being comprised of 35 wt % C_7 asphaltenes. Thus, C_{5-6} asphaltenes and the two co-precipitate fractions obtained from extended solvent extraction of C_7 asphaltenes have near identical monomer ion yields. They are also now known to be composed of predominately island-type structures. The results explain the overwhelming mass spectral support of the island-type asphaltene structural motif; island motifs have a ∼50-fold greater monomer ion yield compared to archipelago motifs from the same sample. Given such a large discrepancy in ionization efficiency between the two structural motifs, the use of mass spectral data, without the prior, careful removal of co-precipitates, to identify the "most abundant" structural motif in asphaltenes is fundamentally flawed. The South American crude oil studied herein contains 6.1% by weight purified C_7 asphaltenes that exhibit abundant archipelago fragmentation patterns.

FUTURE DIRECTIONS

The current results are admittedly for a single crude oil. Multiple crude oils will be required to determine the relative abundance of archipelago/island structural motifs and how it varies with crude oil type. Furthermore, the exact reason for the ∼50-fold decrease in the monomer ion yield for archipelago-type asphaltene compounds is currently unknown. We hypothesize that it is due to their increased aggregation tendency based on previous results.[12] Future experiments will be required to address this issue.

ASSOCIATED CONTENT

Supporting Information

The Supporting Information is available free of charge on the ACS Publications website at DOI: 10.1021/acs.energyfuels.7b02873.

Figure captions for Figures S1−S6 (PDF)

Schematic of the asphaltene purification procedure with associated mass yields (Figure S1) (PDF)

IRMPD FT-ICR mass spectrum of the PAH standard after 4000 ms of irradiation time (Figure S2) (PDF)

IRMPD FT-ICR mass spectrum of the perylene standard after 4000 ms of irradiation time (Figure S3) (PDF)

IRMPD FT-ICR mass spectrum of the coronene standard after 4000 ms of irradiation time (Figure S4) (PDF)

IRMPD FT-ICR mass spectrum of the benzo[*k*]-fluoranthene standard after 4000 ms of irradiation time (Figure S5) (PDF)

DOI: 10.1021/acs.energyfuels.7b02873
Energy Fuels 2017, 31, 13509−13518

IRMPD FT-ICR mass spectrum of the pentacene standard after 4000 ms of irradiation time (Figure S6) (PDF)

AUTHOR INFORMATION

Corresponding Authors

*Telephone: +1-850-644-1319. Fax: +1-850-644-1366. E-mail: rowland@magnet.fsu.edu.

*Telephone: +1-850-644-2398. Fax: +1-850-644-1366. E-mail: rodgers@magnet.fsu.edu.

ORCID

Ryan P. Rodgers: 0000-0003-1302-2850

Notes

The authors declare no competing financial interest.

ACKNOWLEDGMENTS

This work was supported by the National Science Foundation (NSF) Division of Materials Research (DMR-1157490), the Florida State University, the Florida State University Future Fuels Institute, and the State of Florida. The authors thank Don F. Smith and Greg Blakney for help with data calibration and instrument performance and Yuri E. Corilo for PetroOrg software. The authors also thank Logan C. Krajewski for help with laser alignment for IRMPD experiments. The authors give a special thanks to Murray R. Gray for the island and archipelago model compounds and Marianny Y. Combariza for providing the South American crude oil.

REFERENCES

(1) Sheu, E. Y. *Energy Fuels* **2002**, *16*, 74−82.

(2) Ruiz-Morales, Y.; Mullins, O. C. *Energy Fuels* **2009**, *23*, 1169−1177.

(3) McKenna, A. M.; Donald, L. J.; Fitzsimmons, J. E.; Juyal, P.; Spicer, V.; Standing, K. G.; Marshall, A. G.; Rodgers, R. P. *Energy Fuels* **2013**, *27*, 1246−1256.

(4) Strausz, O. P.; Mojelsky, T. W.; Faraji, F.; Lown, E. M.; Peng, P. *Energy Fuels* **1999**, *13*, 207−227.

(5) Mullins, O. C. *Energy Fuels* **2009**, *23*, 2845−2854.

(6) Strausz, O. P.; Safarik, I.; Lown, E. M.; Morales-Izquierdo, A. *Energy Fuels* **2008**, *22*, 1156−1166.

(7) Groenzin, H.; Mullins, O. C. *Energy Fuels* **2000**, *14*, 677−684.

(8) Speight, J. G. *Fuel* **1971**, *50*, 175−186.

(9) Nagy, B.; Gagnon, G. C. *Geochim. Cosmochim. Acta* **1961**, *23*, 155−185.

(10) Ray, B. R.; Witherspoon, P. A.; Grim, R. E. *J. Phys. Chem.* **1957**, *61*, 1296−1302.

(11) Andrews, A. B.; Guerra, R. E.; Mullins, O. C.; Sen, P. N. *J. Phys. Chem. A* **2006**, *110*, 8093−8097.

(12) Groenzin, H.; Mullins, O. C. *J. Phys. Chem. A* **1999**, *103*, 11237−11245.

(13) Mullins, O. C. *Energy Fuels* **2010**, *24*, 2179−2207.

(14) Pomerantz, A. E.; Hammond, M. R.; Morrow, A. L.; Mullins, O. C.; Zare, R. N. *J. Am. Chem. Soc.* **2008**, *130*, 7216−7217.

(15) Pomerantz, A. E.; Hammond, M. R.; Morrow, A. L.; Mullins, O. C.; Zare, R. N. *Energy Fuels* **2009**, *23*, 1162−1168.

(16) McKenna, A. M.; Marshall, A. G.; Rodgers, R. P. *Energy Fuels* **2013**, *27*, 1257−1267.

(17) Hortal, A. R.; Hurtado, P.; Martínez-Haya, B.; Mullins, O. C. *Energy Fuels* **2007**, *21*, 2863−2868.

(18) Miller, J. T.; Fisher, R. B.; Thiyagarajan, P.; Winans, R. E.; Hunt, J. E. *Energy Fuels* **1998**, *12*, 1290−1298.

(19) Trejo, F.; Ancheyta, J. *Ind. Eng. Chem. Res.* **2007**, *46*, 7571−7579.

(20) Poveda, J. C.; Molina, D.; Martinez, H.; Florez, O.; Campillo, B. *Energy Fuels* **2014**, *28*, 735−744.

(21) Strausz, O. P.; Mojelsky, T. W.; Lown, E. M. *Fuel* **1992**, *71*, 1355−1363.

(22) Strausz, O. P.; Peng, P.; Murgich, J. *Energy Fuels* **2002**, *16*, 809−822.

(23) Mullins, O. C. Petroleomics and Structure−Function Relations of Crude Oils and Asphaltenes. In *Asphaltenes, Heavy Oils, and Petroleomics*; Mullins, O. C., Sheu, E. Y., Hammami, A., Marshall, A. G., Eds.; Springer: New York, 2007; Chapter 1, pp 1−16, DOI: 10.1007/0-387-68903-6_1.

(24) Alvarez-Ramírez, F.; Ruiz-Morales, Y. *Energy Fuels* **2013**, *27*, 1791−1808.

(25) Yen, T. F.; Erdman, J. G.; Pollack, S. S. *Anal. Chem.* **1961**, *33*, 1587−1594.

(26) Mullins, O. C.; Sabbah, H.; Eyssautier, J.; Pomerantz, A. E.; Barré, L.; Andrews, A. B.; Ruiz-Morales, Y.; Mostowfi, F.; McFarlane, R.; Goual, L.; Lepkowicz, R.; Cooper, T.; Orbulescu, J.; Leblanc, R. M.; Edwards, J.; Zare, R. N. *Energy Fuels* **2012**, *26*, 3986−4003.

(27) Goual, L.; Sedghi, M.; Wang, X.; Zhu, Z. *Langmuir* **2014**, *30*, 5394−5403.

(28) Tanaka, R.; Sato, E.; Hunt, J. E.; Winans, R. E.; Sato, S.; Takanohashi, T. *Energy Fuels* **2004**, *18*, 1118−1125.

(29) Schuler, B.; Meyer, G.; Peña, D.; Mullins, O. C.; Gross, L. *J. Am. Chem. Soc.* **2015**, *137*, 9870−9876.

(30) Buenrostro-Gonzalez, E.; Groenzin, H.; Lira-Galeana, C.; Mullins, O. C. *Energy Fuels* **2001**, *15*, 972−978.

(31) Tang, W.; Hurt, M. R.; Sheng, H.; Riedeman, J. S.; Borton, D. J.; Slater, P.; Kenttämaa, H. I. *Energy Fuels* **2015**, *29*, 1309−1314.

(32) Pinkston, D. S.; Duan, P.; Gallardo, V. A.; Habicht, S. C.; Tan, X.; Qian, K.; Gray, M.; Mullen, K.; Kenttämaa, H. I. *Energy Fuels* **2009**, *23*, 5564−5570.

(33) Riedeman, J. S.; Kadasala, N. R.; Wei, A.; Kenttämaa, H. I. *Energy Fuels* **2016**, *30*, 805−809.

(34) Sharma, A.; Groenzin, H.; Tomita, A.; Mullins, O. C. *Energy Fuels* **2002**, *16*, 490−496.

(35) Sabbah, H.; Morrow, A. L.; Pomerantz, A. E.; Mullins, O. C.; Tan, X.; Gray, M. R.; Azyat, K.; Tykwinski, R. R.; Zare, R. N. *Energy Fuels* **2010**, *24*, 3589−3594.

(36) Borton, D.; Pinkston, D. S.; Hurt, M. R.; Tan, X.; Azyat, K.; Scherer, A.; Tykwinski, R.; Gray, M.; Qian, K.; Kenttämaa, H. I. *Energy Fuels* **2010**, *24*, 5548−5559.

(37) Apicella, B.; Alfè, M.; Amoresano, A.; Galano, E.; Ciajolo, A. *Int. J. Mass Spectrom.* **2010**, *295*, 98−102.

(38) Sabbah, H.; Morrow, A. L.; Pomerantz, A. E.; Zare, R. N. *Energy Fuels* **2011**, *25*, 1597−1604.

(39) Gray, M.; Tykwinski, R.; Stryker, J.; Tan, X. *Energy Fuels* **2011**, *25*, 3125−3134.

(40) Hosseini-Dastgerdi, Z.; Tabatabaei-Nejad, S.; Khodapanah, E.; Sahraei, E. *Asia-Pac. J. Chem. Eng.* **2015**, *10*, 1−14.

(41) Chacón-Patiño, M. L.; Vesga-Martínez, S. J.; Blanco-Tirado, C.; Orrego-Ruiz, J. A.; Gómez-Escudero, A.; Combariza, M. Y. *Energy Fuels* **2016**, *30*, 4550−4561.

(42) Derakhshesh, M.; Bergmann, A.; Gray, M. R. *Energy Fuels* **2013**, *27*, 1748−1751.

(43) Gawrys, K. L.; Blankenship, G. A.; Kilpatrick, P. K. *Langmuir* **2006**, *22*, 4487−4497.

(44) Rueda-Velásquez, R. I.; Freund, H.; Qian, K.; Olmstead, W. N.; Gray, M. R. *Energy Fuels* **2013**, *27*, 1817−1829.

(45) Ancheyta, J.; Trejo, F.; Rana, M. S. *Asphaltenes: Chemical Transformation during Hydroprocessing of Heavy Oils*; CRC Press: Boca Raton, FL, 2010; DOI: 10.1201/9781420066319.

(46) Savage, P. E.; Klein, M. T.; Kukes, S. G. *Ind. Eng. Chem. Process Des. Dev.* **1985**, *24*, 1169−1174.

(47) Savage, P. E.; Klein, M. T.; Kukes, S. G. *Energy Fuels* **1988**, *2*, 619−628.

(48) Chacón-Patiño, M. L.; Blanco-Tirado, C.; Orrego-Ruiz, J. A.; Gómez-Escudero, A.; Combariza, M. Y. *Energy Fuels* **2015**, *29*, 6330−6341.

(49) Karimi, A.; Qian, K.; Olmstead, W. N.; Freund, H.; Yung, C.; Gray, M. R. *Energy Fuels* **2011**, *25*, 3581−3589.

DOI: 10.1021/acs.energyfuels.7b02873
Energy Fuels 2017, 31, 13509−13518

(50) Gray, M. R. *Energy Fuels* **2003**, *17*, 1566−1569.
(51) Liao, Z.; Zhao, J.; Creux, P.; Yang, C. *Energy Fuels* **2009**, *23*, 6272−6274.
(52) Yasar, M.; Trauth, D. M.; Klein, M. T. *Energy Fuels* **2001**, *15*, 504−509.
(53) Trejo, F.; Ancheyta, J.; Rana, M. S. *Energy Fuels* **2009**, *23*, 429−439.
(54) Alvarez, E.; Marroquín, G.; Trejo, F.; Centeno, G.; Ancheyta, J.; Díaz, J. A. I. *Fuel* **2011**, *90*, 3602−3607.
(55) Rogel, E.; Witt, M. *Energy Fuels* **2017**, *31*, 3409−3416.
(56) Karimi, A.; Qian, K.; Olmstead, W. N.; Freund, H.; Yung, C.; Gray, M. R. *Energy Fuels* **2011**, *25*, 3581−3589.
(57) Gray, M. R.; Le, T.; McCaffrey, W. C.; Berruti, F.; Soundararajan, S.; Chan, E.; Huq, I.; Thorne, C. *Ind. Eng. Chem. Res.* **2001**, *40*, 3317−3324.
(58) Mullins, O. C. *Annu. Rev. Anal. Chem.* **2011**, *4*, 393−418.
(59) Stefan, S. E.; Ehsan, M.; Pearson, W. L.; Aksenov, A.; Boginski, V.; Bendiak, B.; Eyler, J. R. *Anal. Chem.* **2011**, *83*, 8468−8476.
(60) Polfer, N. C.; Valle, J. J.; Moore, D. T.; Oomens, J.; Eyler, J. R.; Bendiak, B. *Anal. Chem.* **2006**, *78*, 670−679.
(61) Podgorski, D. C.; Corilo, Y. E.; Nyadong, L.; Lobodin, V. V.; Bythell, B. J.; Robbins, W. K.; McKenna, A. M.; Marshall, A. G.; Rodgers, R. P. *Energy Fuels* **2013**, *27*, 1268−1276.
(62) Jarrell, T. M.; Jin, C.; Riedeman, J. S.; Owen, B. C.; Tan, X.; Scherer, A.; Tykwinski, R. R.; Gray, M. R.; Slater, P.; Kenttämaa, H. I. *Fuel* **2014**, *133*, 106−114.
(63) Kaiser, N. K.; Quinn, J. P.; Blakney, G. T.; Hendrickson, C. L.; Marshall, A. G. *J. Am. Soc. Mass Spectrom.* **2011**, *22*, 1343−1351.
(64) Blakney, G. T.; Hendrickson, C. L.; Marshall, A. G. *Int. J. Mass Spectrom.* **2011**, *306*, 246−252.
(65) Corilo, Y. E. *PetroOrg Software*; Florida State University: Tallahassee, FL, 2017; http://www.petroorg.com.
(66) Alboudwarej, H.; Beck, J.; Svrcek, W. Y.; Yarranton, H. W.; Akbarzadeh, K. *Energy Fuels* **2002**, *16*, 462−469.
(67) Schuler, B.; Fatayer, S.; Meyer, G.; Rogel, E.; Moir, M.; Zhang, Y.; Harper, M. R.; Pomerantz, A. E.; Bake, K. D.; Witt, M.; Peña, D.; Kushnerick, J. D.; Mullins, O. C.; Ovalles, C.; van den Berg, F. G. A.; Gross, L. *Energy Fuels* **2017**, *31*, 6856−6861.
(68) Ha, J.; Cho, E.; Kim, S. *Energy Fuels* **2017**, *31*, 6960−6967.
(69) Hurt, M. R.; Borton, D. J.; Choi, H. J.; Kenttämaa, H. I. *Energy Fuels* **2013**, *27*, 3653−3658.

■ NOTE ADDED AFTER ASAP PUBLICATION

This article published November 20, 2017 with errors in equation 1. The corrected version published November 21, 2017.

DOI: 10.1021/acs.energyfuels.7b02873
Energy Fuels 2017, 31, 13509−13518